DISSOLUTION OF UO_2 FUEL BY MOLTEN ZIRCALOY-4

P.J. Hayward, I.M. George and M.C. Arneson
Containment Analysis Branch
AECL Research, Whiteshell Laboratories
Pinawa, Manitoba ROE 1LO

INTRODUCTION

Under certain hypothetical CANDU (CANada Deuterium Uranium) accident scenarios involving impaired cooling, rapid core heating to temperatures above the cladding melting point can occur. The molten Zircaloy-4 (Zry) cladding then has the potential of dissolving a significant fraction of the UO_2 fuel, thereby releasing fission products. Before fuel dissolution in molten Zry can proceed, however, initial oxygen diffusion from the fuel and/or from steam into the cladding must occur to allow the molten Zry to wet the fuel [1]. Once fuel dissolution has commenced, the dissolution rate is greatly accelerated by stirring of the melt, e.g., by convection or by gravity-induced movement of the molten cladding over the fuel surfaces [2,3].

Influence of UO_2/Molten-Zry Mass and Surface Area/Volume Ratios

The UO_2/Zry mass ratio in the fuel bundle is an important parameter that indirectly influences the level of fuel solubility in molten cladding. Previous work [3,4] has shown that fuel solubility depends both on temperature and on the O concentration in the melt. The latter originates from the UO_2 by solid-state O diffusion and by subsequent fuel dissolution in the melt if no other O sources (e.g., steam) are available.

Assuming good cladding/fuel contact during the temperature transient, O will diffuse from fuel to cladding, dissolving in the Zry and reducing the fuel to UO_{2-x}. The solubility of O in Zr increases from ~29 at.% at room temperature to ~35 at.% at the melting point of O-saturated Zr [5]. Thus, the cladding can gain up to ~35 at.% O before melting, and the extent of fuel reduction (i.e., the value of x in UO_{2-x}) is determined by the UO_2/Zry mass ratio. Subsequent UO_{2-x} dissolution gives further O enrichment of the melt. Hence, the final melt O content and, thus, the fuel solubility, depends in part on the initial UO_2/Zry mass ratio.

The <u>rate</u> of fuel dissolution in molten Zry is directly controlled by the fuel surface area/molten Zry volume (SA/V) ratio. The dissolution reaction may be approximated as:

(1) $$\underset{\text{(solid)}}{UO_2} + \underset{\text{(liquid)}}{Zr} \longrightarrow \underset{\text{(liquid)}}{(U,Zr)O_{2-x}}$$

If first- order reaction kinetics are assumed, the rate of change of the UO_2 concentration in solution (C_t) at time t will be directly proportional to the degree of undersaturation, i.e.,

(2) $$dC_t/dt = k'(C_s - C_t)$$

where C_s is the concentration at saturation and k' is given by $k' = k.(SA/V)$, where k is the rate constant. Hence, k' and dC_t/dt increase proportionately with SA/V. From Equation (2), it is easily shown that

$$C_t = C_s(1 - e^{-k't}). \tag{3}$$

To place the above remarks in context, consider the mass and SA/V ratios in clad Pickering A and Bruce A fuel (ignoring all Zry in the bundle except for the fuel sheathing). The mass ratios are 13.0 and 10.9 respectively. The initial SA/V ratio for clad Pickering A fuel is ~2300 m^{-1}, falling to an estimated ~1400 m^{-1} after relocation of the molten cladding into the bundle subchannels [6]. Cladding relocation in Bruce A fuel would also cause a similar SA/V reduction from the initial value of ~2290 m^{-1}.

Thus, it is important to use realistic values for the mass and SA/V ratios in designing CANDU-relevant dissolution experiments. Because of geometric constraints, however, it is impossible to match both the mass and SA/V ratios of clad CANDU fuel with one crucible/Zry-charge configuration. Consequently, the experiments described below and reported earlier [4] involve different crucible sizes and/or Zry masses to simulate either the SA/V ratio after cladding relocation or the UO_2/Zry mass ratio.

Previous Investigations

Laboratory studies of UO_2/molten-Zry dissolution have previously been reported by Hofmann and co-workers [1,7], Kim and Olander [3] and Hayward et al.[4]. In all cases, the experiments involved rapid heating of Zry samples in UO_2 crucibles under argon atmospheres to selected temperatures, holding each sample at the chosen temperature for a known time interval before cooling and chemical analysis of the central melt region. Kim and Olander and Hayward et al., using direct analysis methods on samples from tests in the temperature range 1950-2400°C, observed rapid melt saturation with respect to UO_2. However, Hofmann et al., using an indirect analytical method, found no evidence of UO_2 melt saturation during tests in the temperature range 1950-2250°C. Possible reasons for this disagreement are discussed later in this paper.

Scope of Present Experiments

This paper describes and discusses the results of UO_2 dissolution experiments in nominally O-free Zry at 2000 and 2200°C. In each test, a UO_2/Zry mass ratio of ~10.9 has been used to simulate the relative masses in Bruce fuel bundles [8]. UO_2 solubilities as functions of temperature at this mass ratio have been determined from analyses of the melt regions. The solubilities have been compared with earlier results obtained using different mass and SA/V ratios at temperatures up to 2400°C, with either initially O-free Zry or Zry containing ~25 at.% O as the reactant [4]. The Zry/25 at.% O was used to represent the O-saturated Zry component of steam-oxidized cladding.

EXPERIMENTAL

UO_2 crucibles were formed by machining Bruce-type UO_2 pellets (~16.6 mm long, ~12.1 mm-diameter) to remove an axial core of ~6.7 mm-diameter and ~13 mm long. Before use, each ~14.8-g crucible was cleaned ultrasonically to remove loose UO_2 particles. Cylindrical Zry samples were machined from Teledyne Wah Chang bar stock to fit the crucibles, with a UO_2/Zry mass ratio of ~10.9. The O-content of the Zry bar stock was quoted by the suppliers as ~0.1 wt.%.

In each test, the crucible plus Zry charge was contained within a ThO_2 crucible (to catch any melt spillage) and placed in the hot zone of a Centorr tungsten resistance furnace. The furnace was coupled to a programmable controller via a type C thermocouple. After thorough purging of the furnace with high-purity argon, the sample was heated to ~1550°C and allowed to equilibrate at this temperature for ~3 min. The sample was then heated to the test temperature (2000 or 2200°C) at ~7°C/s, with the heating rate falling close to the set point. The sample was held for the desired time (0-15 min) at this temperature and then cooled rapidly (~4°C/s) to 1450°C, with final slow cooling to room temperature. The sample temperature was continuously recorded during each test using a dual-wavelength pyrometer focussed on the Zry charge through a fused quartz window in the furnace roof. A second pyrometer, focussed on the ThO_2 crucible through a furnace side-wall window, was used as a check on the sample temperature.

After each test, the sample was sectioned along the cylindrical axial plane to expose the solidified melt region. One half of each sample was used for scanning electron microscope - energy dispersive X-ray (SEM/EDX) analyses, employing backscattered electron images to give maximum phase contrast. The other half was used for inductively coupled plasma (ICP) emission spectrometry analysis of the melt. Reference 4 gives full details of the experimental and analytical methods and of analytical error computations.

RESULTS

ICP Spectrometry Analyses

Because of uncertainty in melt O concentrations (obtained from ICP analyses by difference), UO_2 concentrations for each melt are reported and discussed below in terms of the U/(U + Zr) wt.% ratio, i.e., on an O-free basis. The mean results from ICP analyses of duplicate melt samples from each of the 2000°C and 2200°C test specimens are plotted against $t^{0.5}$ in Figure 1. Also shown are curves representing the best-fit lines from Equation (3) to the data at these temperatures. Melt saturation is seen to occur rapidly at both temperatures, with C_s values of ~37% at 2000°C and ~70% at 2200°C.

Since UO_2 dissolution in molten Zry is so rapid, the quantity dissolved during the ramp between the Zry melting point and each isotherm temperature is not negligible. Hence, the start of each test has been taken as the time at which the Zry charge melted; this time was clearly evident as a discontinuity in each pyrometer time/temperature trace. Errors in estimation of t by this procedure are relatively small at longer times, but may be important in modeling the early stages of dissolution. Thus, the rate constant (k) values shown in Figure 1 should be regarded as approximate since the shape of the fitted curve from Equation (3) is disproportionately influenced by k at short times.

SEM/EDX Analyses of 2000°C Samples

Figure 2(a) shows the post-test crucible microstructure of a ~15-min test sample in a region ~1 mm from the melt/crucible interface. All specimens had similar crucible microstructures, as did those from earlier experiments [4]. The bright spots in the image are U metal precipitates, formed at UO_2 grain boundaries and generally distributed uniformly throughout the undissolved crucible material. However, except for a thin band at the melt/crucible interface, the precipitates were invariably absent from the ~30-μm-wide crucible zone adjacent to the melt.

The melt regions in all 2000°C samples where UO_2 saturation had been reached (i.e., from tests of over ~100-s duration) showed very similar dendritic microstructures and phase compositions. The melt/crucible interface was usually marked by a transition zone of average thickness ~100 μm. This zone, which occupied a negligible fraction of the total melt volume, consisted of ceramic phase(s) of mean composition $[U_{0.39} \cdot Zr_{0.61}]O_{1.5\pm0.2}$.

The melt microstructures were basically two-phase, consisting of uniformly distributed U-rich and Zr-rich regions (the light- and dark-coloured phases respectively in Figure 2(b)). Fine-scale exsolution of U-rich precipitates in the Zr-rich regions and of Zr-rich precipitates in the U-rich regions had also occurred.

The mean compositions of the U-rich and Zr-rich major phases were derived from duplicate EDX analyses for U, Zr and Sn made at five widely separate sites within each specimen, with approximate values for O being obtained by difference. In selecting regions for analysis, care was taken to avoid including any exsolved precipitates. Although a few of the U-rich precipitates were of sufficient size (~1 μm) for EDX analysis, the Zr-rich precipitates were invariably too small.

The analyses for each of the two major phases in all samples showing UO_2 saturation were very similar, with mean compositions being (i) a $[U_{0.88\pm0.05} \cdot Zr_{0.12\pm0.05}]\ O_{1.80\pm0.13}$ ceramic phase, and (ii) a metallic phase, corresponding closely to O-saturated Zr containing traces of U and Sn. The exsolved U-rich precipitates within the O-saturated Zr phase were almost pure U metal.

SEM/EDX Analyses of 2200°C Samples

The melt regions of the 9 samples from 2200°C tests of ≥2-min duration (i.e., samples close to, or at, UO_2 saturation) exhibited almost identical microstructures and an overall dendritic mode of crystallization. The microstructures were also very similar to those of the 2000°C UO_2-saturated samples, except for a greater abundance of the U-rich ceramic phase (see Figure 2(c)), as would be expected from the higher U contents of the 2200°C melts. As before, fine-scale U-rich precipitates in the Zr-rich major phase and Zr-rich precipitates in the U-rich major phase were seen.

The melt/crucible interfaces in the 2200°C specimens were much sharper than in the 2000°C specimens (see Figure 2(d)). Uranium metal precipitates were again found throughout the undissolved crucible material and in a thin band at the melt/crucible interface, but were absent from the ~30-μm-wide crucible zone adjacent to the melt.

Duplicate EDX analyses were made for each phase at five widely separate sites within the melt regions of the samples showing UO_2 saturation (i.e., produced in ≥3-min tests). Each phase type gave similar analyses except for somewhat variable values for oxygen. Overall mean compositions were (i) $[U_{0.86\pm0.03}\cdot Zr_{0.14\pm0.03}]O_{1.56\pm0.44}$ for the ceramic phase, and (ii) O-saturated Zr containing traces of U and Sn for the metallic phase. The minor U-rich precipitates within the O-saturated Zr phase were almost pure U metal.

DISCUSSION

Origin of U Metal Droplets in Undissolved Crucible Material

The origin of the U metal precipitates in the undissolved crucible after each test is indicated by the U-O phase diagram [9]. Rapid diffusion of O from UO_2 to Zry above ~1100°C will reduce the crucible either to substoichiometric UO_{2-x}, or, with further O-diffusion, to $[U_{liq} + UO_{2-x}]$. In the former case, molten U will be continuously precipitated when the crucible composition during cooling reaches the $[U_{liq} + UO_{2-x}]$ phase boundary. Thus, at room temperature, the final crucible composition will be stoichiometric UO_2 containing exsolved U. However, if high-temperature O-diffusion moves the crucible composition to within the $[U_{liq} + UO_{2-x}]$ phase field, U liquid will form within the UO_{2-x} structure during the test isotherm, with further disproportionation of UO_{2-x} into U + UO_2 during cooling. In either case, the final crucible composition will be UO_2 with U metal precipitates exsolved at the UO_2 grain boundaries (Figure 2(a)).

As noted above, the U precipitates were always absent from the ~30-μm-wide crucible zone adjacent to the melt, except for a thin layer occurring at the crucible/melt interface. This phenomenon has been seen previously [3,4,7,10] and is attributed by Hofmann [10] to local migration of molten U into the melt via interconnected pores and grain boundaries. An alternative explanation [3] involves melt penetration into the crucible along grain-boundaries, causing assimilation of the U metal precipitates plus further UO_{2-x} to form a single $(U,Zr)O_{2-x}$ phase containing enough Zr^{4+} to stabilize it during cooling to room temperature. However, neither explanation accounts for the thin layer of U metal at the crucible/melt interface, and further work is required for a more complete understanding.

Fuel Solubility and Crystallization Sequence in 2000°C Melts

The occurrence of UO_2 melt saturation at 2000°C and subsequent formation of basically two-phase microstructures during cooling are best understood from the 2000°C U-Zr-O phase diagram section [11] and the quasi-binary UO_2-Zr(O) phase diagram [12], shown in Figures 3 and 4 respectively. Neither diagram represents the true experimental conditions exactly since the minor Zry alloy components, which may alter phase-boundary locations, are not included. Also, the $ZrO_{0.43}$ component in Figure 4 only represents O-saturated Zr below ~1500°C; at higher temperatures, oxygen solubility increases to ~35 at.% at the Zr(O) melting point of 2065°C [5]. Figure 3, however, allows for varying O concentrations, e.g., by O diffusion from UO_2 to the melt, to be considered.

If solid-state O diffusion from fuel to cladding did not occur during heating (e.g., from poor fuel/cladding contact and/or very rapid heating), the reaction path during fuel dissolution would follow the dashed line AB joining Zr and UO_2 in Figure 3. Thus, UO_2 would dissolve until the intersection of AB with the two-phase $[(U,Zr)O_{2-x} + L]$ boundary was reached at Y, when dissolution would cease. Point Y has a U/(U + Zr) wt.% ratio of ~51, the saturation solubility under these conditions. Conversely, with good fuel/cladding contact and slow heating to allow full O saturation of the Zry before melting, the reaction path would follow the dashed line CD joining Zr(O) to UO_{2-x}, where x is determined by the UO_2/Zry mass ratio. Saturation would occur at the intersection of CD with the two-phase boundary at X. Point X has a U/(U + Zr) wt.% ratio of ~30 when the mass ratio is 10.9.

Thus, the compositions at X and Y represent the range limits at this mass ratio for UO_2 solubility in molten Zry at 2000°C. The measured solublity in the present experiments, calculated from the ICP analyses, plots between X and Y on the phase boundary at point Z. The location of Z suggests a curved reaction path (shown schematically in Figure 3) as a result of varying and unequal rates of O and U assimilation by Zry during dissolution.

The $[U_{0.85}\cdot Zr_{0.15}]O_{1.85}$ primary crystallization phase formed on cooling the UO_2-saturated 2000°C melts is shown in Figure 3 as point V. Thus, the tie line across the two-phase region is VZ and the residual melt composition will move <u>initially</u> towards W during cooling, changing direction at lower temperatures in accord with phase-boundary movements.

The origin of the room-temperature microstructure for each melt is evident from Figure 4. Here, point D represents the saturation composition at 2000°C. During cooling to the eutectic temperature, E, the $(U,Zr)O_{2-x}$ phase precipitates until, at E, complete solidification occurs with formation of further $(U,Zr)O_{2-x}$ and α-Zr(O) in proportions given by the lever rule. The diagram also predicts exsolution during further cooling of $(U,Zr)O_{2-x}$ in the α-Zr(O) phase (cooling path F → G) and of α-Zr(O) in the $(U,Zr)O_{2-x}$ phase (cooling path H → I). While these phases may have been present, they were too small for EDX analysis. The observed precipitation of U metal droplets in the α-Zr(O) phase is presumably a lower temperature phenomenon.

<u>Fuel Solubility and Crystallization Sequence in 2200°C Melts</u>

Detailed U-Zr-O phase relations above 2000°C have not been determined, although the two-phase $[(U,Zr)O_{2-x} + L]$ field width is thought [4,13] to shrink at higher temperatures. It is reasonable to suppose that UO_2 melt saturation at higher temperatures occurs by the same mechanism as at 2000°C, viz., by intersection of the reaction path with the two-phase boundary. Thus, the increased UO_2 saturation solubility value of ~70% at 2200°C, compared with ~37% at 2000°C, is caused by contraction of the two-phase field at the higher temperature.

The crystallization path of UO_2-saturated 2200°C melts during cooling is similar to that of corresponding melts at 2000°C. Thus, cooling to E in Figure 4 causes precipitation of $(U,Zr)O_{2-x}$ until, at E, complete solidification occurs with formation of α-Zr(O) and additional $(U,Zr)O_{2-x}$. The greater abundance of the $(U,Zr)O_{2-x}$ phase in the 2200°C sample micrographs, compared with those of 2000°C samples, is the result of higher UO_2 contents in the 2200°C saturated melts. Further cooling below E causes exsolution of $(U,Zr)O_{2-x}$ in the α-Zr(O) phase and of α-Zr(O) in the $(U,Zr)O_{2-x}$ phase. As noted above, the observed formation of U-metal droplets in the α-Zr(O) phase is probably a lower temperature phenomenon.

Comparison with Previous Results

From the above discussion, it is evident that UO_2 solubility in molten Zry should vary inversely with the melt O content at a given temperature. Because a low UO_2/Zry mass ratio produces a relatively high degree of UO_2 reduction from initial O diffusion to the Zry (i.e., a high value of x in UO_{2-x}), subsequent UO_{2-x} dissolution will form a melt of relatively low O content. Hence, UO_2 solubilities should be increased at low UO_2/Zry mass ratios. This prediction is supported by comparison of the present 2000°C saturation value of ~37%, obtained using a UO_2/Zry mass ratio of ~10.9, with that of ~43% obtained earlier [4] using a mass ratio of ~7.1. Further support comes from comparison of the previously measured [4] UO_2 solubilities at ~2350°C of ~78% in initially O-free Zry and of ~66% in Zry/25 at.% O.

UO_2 solubilities in molten Zry are known to increase with rising temperature [3,4,7]. This is illustrated by comparing the present measured values in initially O-free Zry of ~37% at 2000°C and ~70% at 2200°C with the earlier measured value of ~78% at 2350°C [4]. The increase is attributed to progressive contraction of the $[(U,Zr)O_{2-x} + L]$ phase field at higher temperatures, as discussed above.

The saturation values of ~37% at 2000°C and ~70% at 2200°C are in almost exact agreement with Kim and Olander's data at these temperatures [3]. The 2000°C value corresponds to 6.1 vol.% dissolution of Bruce fuel, close to the value of ~6 vol.% measured by Rosinger et al. at 2000°C using internally heated fuel element simulators [14]. The 2200°C value corresponds to 24.3 vol.% dissolution of Bruce fuel.

As noted previously, Hofmann et al. [7] did not observe melt saturation in 1950-2250°C dissolution experiments using unspecified UO_2/Zry mass ratios and SA/V ratios of ~385 m^{-1}. Since their SA/V ratios were approximately one-half that of the present tests, slower dissolution rates would be expected in their experiments, so that saturation may not have been reached in the time allowed. A further reason for the disagreement may lie in their use of an indirect analysis method, which involved correlation of the microstructures of their dissolution test samples with those of standards produced by arc-melting mixtures of UO_2 and Zry under argon. This method fails to account for O-diffusion from undissolved UO_2 crucible material into the melt. As noted above, however, variable melt O-contents can significantly influence UO_2 solubilities and melt microstructures.

CONCLUSIONS

Based on our present results and those of previous experiments [4], we conclude that the saturation solubility of UO_2 in molten Zry varies directly with temperature and inversely with the melt O concentration. The latter is determined by the fuel/cladding mass ratio when external sources of oxygen (e.g., steam) are absent.

The following UO_2 solubilities (U/(U + Zr) wt.% ratio) at saturation have been measured:
(i) ~37% in initially O-free Zry at 2000°C, mass ratio ~10.9;
(ii) ~43% in initially O-free Zry at 2000°C, mass ratio ~7.1;
(iii) ~70% in initially O-free Zry at 2200°C, mass ratio ~10.9;
(iv) ~78% in initially O-free Zry at ~2350°C, mass ratio ~45; and
(v) ~66% in O-rich Zry (Zry/25 at.% O) at ~2350°C, mass ratio ~75.

ACKNOWLEDGEMENTS

We thank P.M. Mathew, D.G. Evans and H.E. Rosinger for useful manuscript reviews and K. Wazney for the ICP analyses.

REFERENCES

1. W. DIENST, P. HOFMANN AND D.K. KERWIN-PECK, "Chemical Interactions Between UO_2 and Zircaloy-4 from 1000 to 2000°C", Nucl. Technol. 65, 109-124, 1984.

2. D.G. EVANS, "A Literature Review of High-Temperature Reactions Between UO_2 and Zircaloy-4," Atomic Energy of Canada Limited Restricted Report, COG-89-126, 1989.

3. K.T. KIM AND D.R. OLANDER, "Dissolution of Uranium Dioxide by Molten Zircaloy II. Convection-Controlled Reaction", J. Nucl. Mater. 154, 102-115, 1988.

4. P.J. HAYWARD, I.M. GEORGE AND M.C. ARNESON, "Dissolution of UO_2 Fuel by Molten Zircaloy Cladding", Atomic Energy of Canada Limited Restricted Report, COG-92-50, 1992 March.

5. R.J. ACKERMANN, S.P. GARG AND E.G. RAUH, "High-Temperature Phase Diagram for the System Zr-O", J. Amer. Ceram. Soc. 60, 341-345, 1977.

6. P.M. MATHEW, D.G. EVANS AND P.J. HAYWARD, unpublished work, 1992.

7. P. HOFMANN, H. UETSUKA, A.N. WILHELM AND E.A. GARCIA, "Dissolution of Solid UO_2 by Molten Zircaloy and Its Modelling", *In* Proceedings IAEA/NEA Symposium on Severe Accidents in Nuclear Power Plants, Sorrento, 1988, IAEA-SM-296/1, 3-17 (1988).

8. J.L. CROSTHWAITE, "CANDU Irradiated-Fuel Handbook", Atomic Energy of Canada Limited Restricted Report, WNRE-371, 1979.

9. E.M. LEVIN AND H.F. MCMURDIE, "Phase Diagrams for Ceramists, 1975 Supplement", Figure 5028B, American Ceramic Society, Westerville, OH, 1975.

10. P. HOFMANN, personal communication, 1991.

11. P. HOFMANN AND C. POLITIS, "The Kinetics of the Uranium Dioxide-Zircaloy Reactions at High Temperatures", J. Nucl. Mater. 87, 375-97, 1979.

12. A. SKOKAN, "High Temperature Phase Relations in the U-Zr-O System", In Proceedings of the Fifth International Meeting on Thermal Nuclear Reactor Safety, Kernforschungszentrum Karlsruhe Report, KfK-3880/2, 1984.

13. D.L. HAGRMAN, "Zircaloy-UO_2-Steam Interactions", EG & G Idaho, Inc., Report No. SE-RSTD-85-010, 1985.

14. H.E. ROSINGER, R.K. RONDEAU, K. DEMOLINE AND K.J. ROSS, "The Interaction and Dissolution of Solid UO_2 by Molten Zircaloy-4 Cladding in an Inert Atmosphere or Steam", In Proceedings 6th Canadian Nuclear Society Conference, Ottawa, 1985, 16.33-16.38.

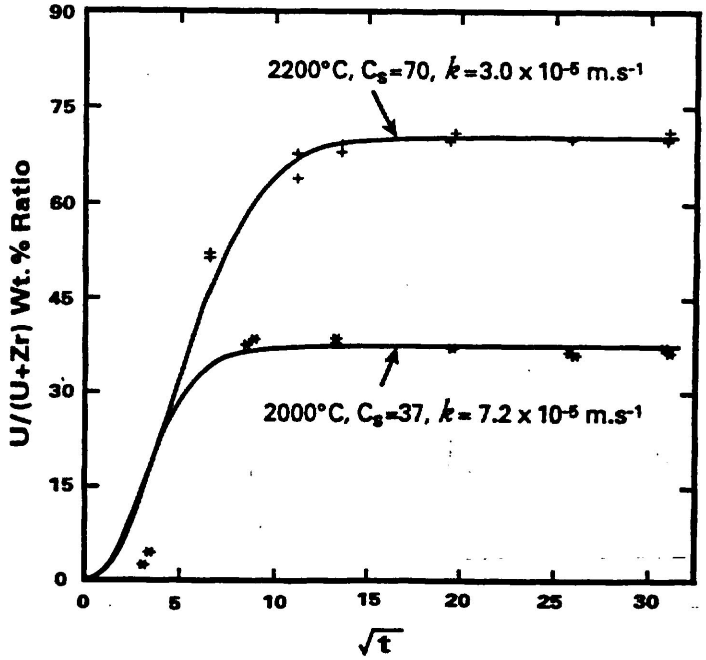

Figure 1: UO_2 Solubilities at 2000°C and 2200°C, Showing Best-Fit Curves from Equation (3)

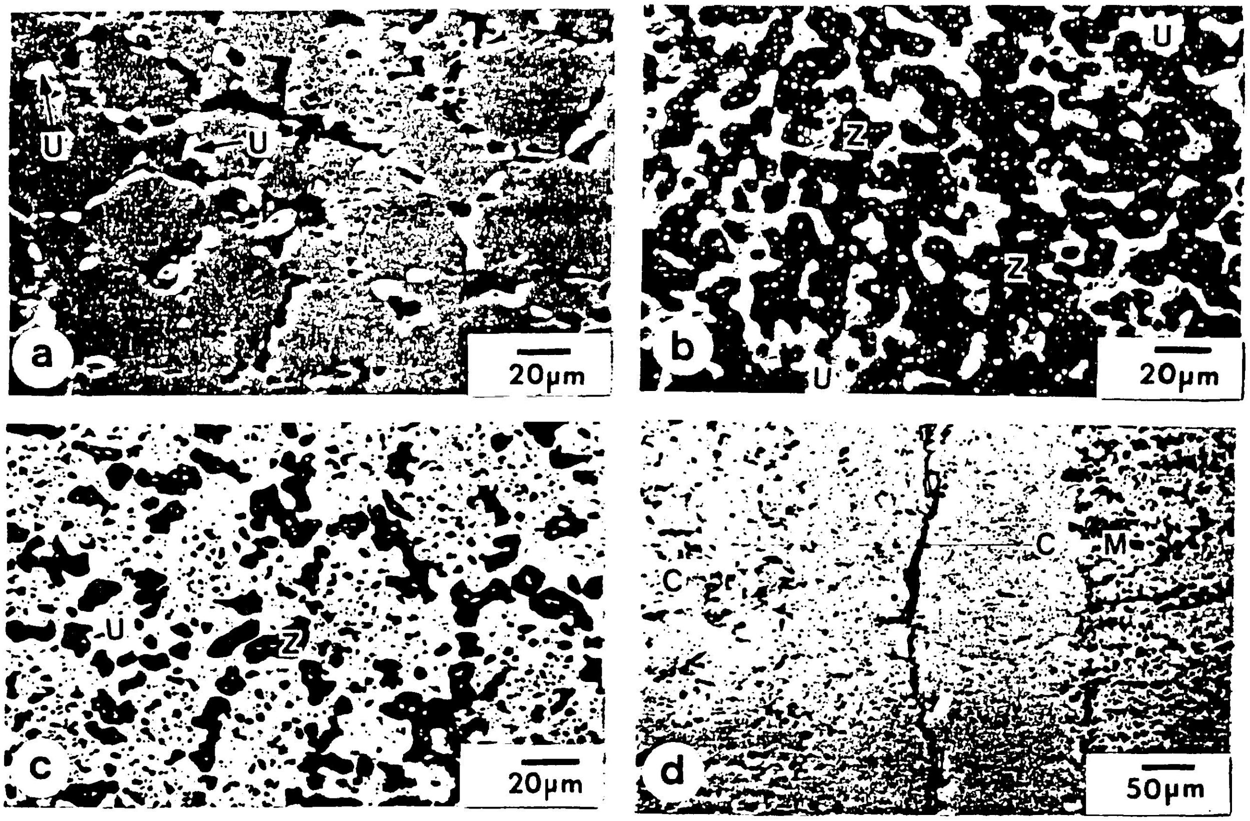

Figure 2. SEM Micrographs of Dissolution Test Specimens: (a) residual crucible microstructure, showing U metal droplets (U); (b) 2000°C specimen melt zone showing U-rich (U) and Zr-rich (Z) major phases and exsolved minor phases; (c) 2200°C specimen melt zone showing U-rich (U) and Zr-rich (Z) phases and exsolved minor phases; and (d) 2200°C transition from melt (M) to crucible(C) showing unequal U droplet distribution close to the interface.

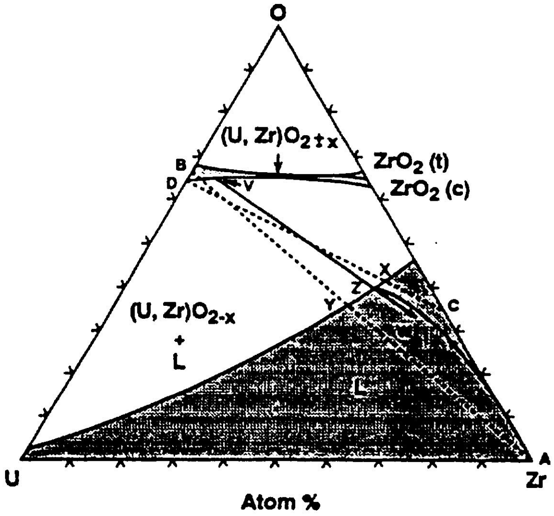

Figure 3. U-Zr-O Phase Diagram at 2000°C. See text for labelling.

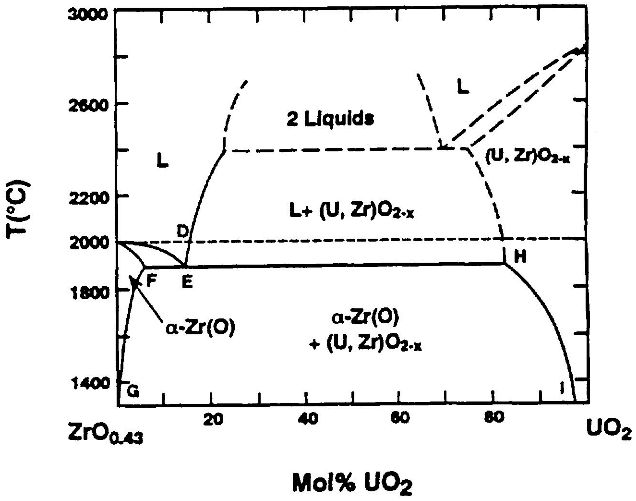

Figure 4. Zr(O)-UO_2 Quasi-Binary Phase Diagram. See text for labelling.